10^{th} International Conference on Fracture Mechanics of Concrete and Concrete Structures
FraMCoS-X
G. Pijaudier-Cabot, P. Grassl and C. La Borderie (Eds)
https://doi.org/10.21012/FC10.234933

MULTISCALE MODELLING OF ION TRANSPORT AND ASR INDUCED DAMAGE IN CONCRETE STRUCTURES

T. ISKHAKOV, J. J. TIMOTHY AND G.MESCHKE

Ruhr University Bochum
Bochum, Germany
e-mail: tagir.iskhakov@rub.de

Key words: Moisture and Ion Transport, Alkali-Silica Reaction, Micromechanics

Abstract. Alkali-Silica Reaction (ASR) is a detrimental expansive reaction in concrete structures, such as dams and pavements, which substantially limits their structural lifetime. Silica present in the so-called "reactive" aggregates reacts with calcium, hydroxyl and alkali ions of the pore fluid to form a hydrophilic alkali-silica gel. The gel fills pre-existing microcracks in the aggregates and the cement paste and swells in the presence of moisture. The gel pressure induced microcrack growth manifests itself as an expansion at the macroscale. The so-called *slow-late* ASR damage mechanism initiates at the aggregate scale, leading to concrete degradation in the form of microcracks, which starts in the aggregates and eventually propagates into the cement paste. In order to predict damage and expansion profiles in a concrete pavement a multiscale approach is adopted. The microcracking process that is characterized by linear elastic fracture mechanics and microporomechanics is upscaled by means of mean-field homogenization. Moisture and alkali transport in intact and damaged concrete at the macroscale as well as the diffusion of alkali ions into the aggregate at the microscale is also considered in the model to account for the influence of external alkali and moisture supply on the durability of concrete pavements. The capabilities of the multiscale chemo-mechanical model at different scales are illustrated by comparison with experimental measurements.

1 INTRODUCTION

Under specific humidity and temperature conditions, concrete structures containing reactive aggregates are susceptible to damage induced by the Alkali-Silica Reaction (ASR). This reaction between silica in the aggregates, calcium and alkali results in the formation of an alkali-silica gel. The gel diffuses through the concrete microstructure filling existing flaws and voids and subsequently generating an internal pressure. This pressure leads to microcracking and expansion of concrete reducing its load carrying capacity and service life. In our work we investigate the influence of external alkali supply, in the form of de-icing salts, on concrete pavement degradation and expansion.

In Section 2 we present and calibrate the model describing moisture and external alkali transport into the concrete pavement. In Section 3 we review the ASR kinetics and ASR induced deterioration modelling approaches developed in [5] and [4], respectively. Finally, in Section 4 we combine all three models together in order to obtain the evolution of microcrack propagation and strains in a concrete pavement. In Section 5 we summarize the results and provide conclusions.

2 MASS TRANSPORT IN CONCRETE

2.1 Moisture transport

Characterizing moisture content, its spatial distribution and evolution is a fundamental in-

gredient in modeling the development of ASR especially in concrete structures exposed to wet environmental conditions, since sufficient moisture content is a pre-requisite for the ASR gel to swell. Furthermore, the presence of moisture is also necessary for the transport of ions through the pore-space in concrete. Mass conservation describing the movement of the liquid phase in unsaturated cementitious materials is formulated as [2]

$$\frac{\partial \theta}{\partial t} - \nabla \cdot (D_\theta \nabla \theta) \;=\; 0, \qquad (1)$$

where t is the time and θ is the moisture content, which is defined as the fractional volume of water whose maximum possible value is the concrete porosity, i.e. $\theta \in [0, \phi]$. $\theta = 0$ and $\theta = \phi$ define fully dry and fully saturated conditions, respectively. $0 < \theta < \phi$ characterizes the state when the liquid phase occupies only a fraction of the total porous volume. D_θ in Eq.(1) is the moisture diffusivity:

$$D_\theta(\theta) \;=\; \frac{K(\theta)}{\frac{\partial \theta}{\partial h}}. \qquad (2)$$

Here h is the capillary pressure head while $K(\theta)$ is the hydraulic conductivity given by

$$K = \;\; K_r(\theta) K_s. \qquad (3)$$

where K_r is the dimensionless relative hydraulic conductivity and K_s is the hydraulic conductivity for fully saturated, undamaged porous medium.

According to the van Genuchten model [8] used here, the retention curve, representing the relation between the effective saturation S_e and the capillary head h, is given by

$$S_e = \left(1 + (\alpha |h|)^{\frac{1}{1-m}}\right)^{-m}, \; 0 < m < 1, \quad (4)$$

where α is a characteristic parameter. The effective saturation S_e is also known as the normalized moisture content and can be calculated by

$$S_e \;=\; \frac{\theta - \theta_r}{\theta_s - \theta_r}, \qquad (5)$$

in which θ_s is the moisture content corresponding to the fully saturated state, i.e. equal to the porosity ϕ, and θ_r is the moisture content corresponding to the dry state. The relative hydraulic conductivity is found as

$$K_r = S_e^l \left(1 - \left(1 - S_e^{\frac{1}{m}}\right)^m\right)^2, \; 0 < m < 1. \quad (6)$$

The parameter l is set to $l = 0.5$ for cementitious materials [1, 7], and the parameters α and m are chosen as $\alpha = 7.55 \cdot 10^{-4}\,[1/m]$ and $m = 0.25$ to fit the water retention curve obtained experimentally [10] as part of the project FOR 1498.

2.2 Ion transport

Alkali ions are one of the main reactants in ASR. Thus, its concentration affects the reaction process and the formation of the ASR gel [5]. In the winter period additional supply of alkali ions in the form of the de-icing salts on the pavement surface may lead to a larger expansion of the formed ASR gel and consequently to higher deterioration and expansion of concrete. In the following it is assumed that the transport of alkalis from the concrete surface into the bulk material is predominantly driven by advection

$$\frac{\partial (\theta c)}{\partial t} - \nabla \cdot (c D_\theta \nabla \theta) \;=\; 0, \qquad (7)$$

where c is the ion concentration. Inserting Eq.(1) into Eq.(7) we obtain

$$\frac{\partial c}{\partial t} \;=\; \beta \frac{D_\theta \nabla \theta}{\theta} \nabla c, \qquad (8)$$

where coefficient β is introduced to account for the retardation of ion transport in the fine pores of the hardened cement paste [2, 11]. In order to avoid numerical oscillations Eq.(8) is solved using the first-order upwind scheme

$$c_i^{k+1} = c_i^k - \Delta t a \frac{c_i^k - c_{i-1}^k}{\Delta x}, \text{ for } a > 0, \qquad (9)$$

$$c_i^{k+1} = c_i^k - \Delta t a \frac{c_{i+1}^k - c_i^k}{\Delta x}, \text{ for } a < 0, \quad (10)$$

where $a = -\beta \left[\frac{D_\theta \nabla \theta}{\theta}\right]_i^k$ defines the velocity of the moisture flow, and i and k are the indices in the discretized space and time domain, respectively.

2.3 Capillary suction in a concrete prism

We calibrate and validate the model describing moisture and ion transport in partially saturated concrete pavement using the results from the experimental research [9] performed within the project FOR 1498. In the laboratory tests, concrete prisms of size $27 \times 12 \times 14\,[cm]$ were cut out of a beam of size $27 \times 300 \times 50\,[cm]$ in lateral direction. One end of the concrete prisms - the lower surface - was submerged into 3.6 wt.-% NaCl solution. The ingress of the moisture into the concrete due to capillary suction was determined using TDR measurement.

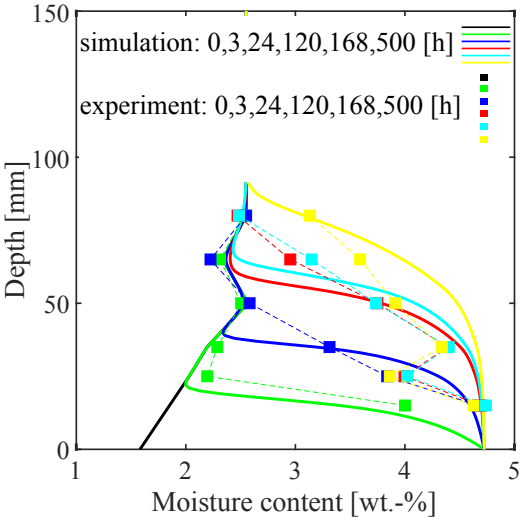

Figure 1: Moisture profiles in undamaged concrete specimen after 0, 3, 24, 120, 168 and 500 hours: Comparison of experimental measurements and model predictions.

The point data in Fig.(1) denotes experimentally measured profiles of moisture in the prism after 0, 3, 24, 120, 168 and 500 hours. The solid lines denote the model prediction. The modelled profiles take into account the cracks in the beam of size $27 \times 300 \times 50\,[cm]$ which are formed close to the surface of the beam due to its drying and shrinkage using a non-linear hydraulic conductivity K_s as shown in Fig.(2).

Additionally, the absorption of water using the gravimetric analysis was determined experimentally [9] and compared with the model predictions as shown in Fig.(3).

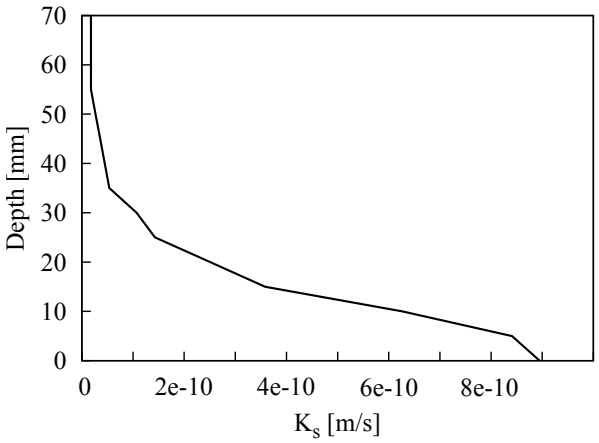

Figure 2: Variation of the hydraulic conductivity K_s along the depth of the beam

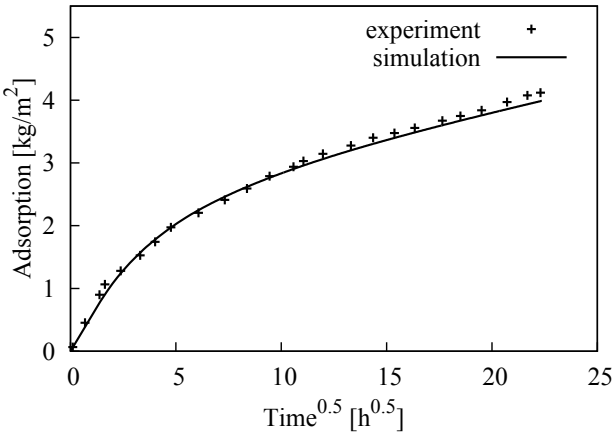

Figure 3: Model predictions and experimental measurements of moisture uptake by the concrete prism.

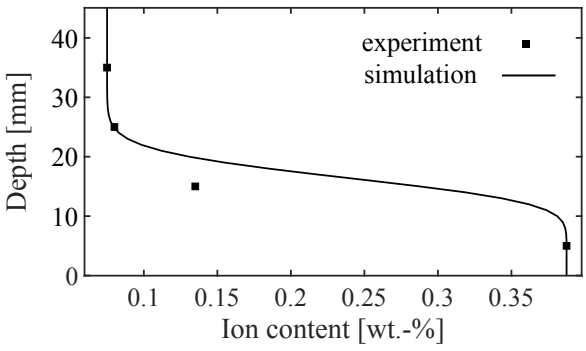

Figure 4: Model predictions and experimental measurements of sodium ion concentration along the depth of a concrete prism after 500 hours.

The profiles of alkali ion concentration along the depth of the concrete prism were determined by wet chemistry analysis [9]. Fig.(4) presents the comparison of the experimental and model predictions for ion content along the depth of the concrete prism.

3 MICROMECHANICAL MODELLING OF ASR

Given the amount of the moisture and sodium ion concentration at a certain depth of the pavement, the gel formation at the concrete mesoscale is modelled. The kinetics of ASR is governed by the transport of alkali ions into the reactive aggregate which is characterized by Fick's law in spherical coordinates [5]

$$\frac{\partial c_{agg}}{\partial t} = D_{agg}\left(\frac{2}{r}\frac{\partial c_{agg}}{\partial r} + \frac{\partial^2 c_{agg}}{\partial r^2}\right), \quad (11)$$

where D_{agg} is the diffusivity of the aggregate, c_{agg} is the sodium concentration at the scale of aggregate which is depicted in Fig.(5).

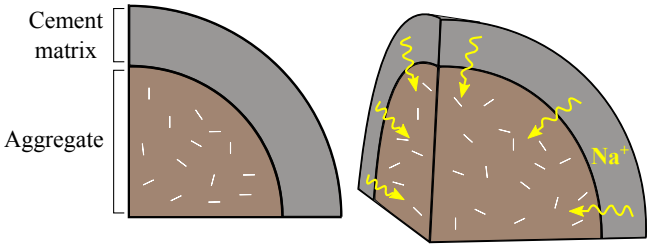

Figure 5: Mesoscale geometry used for the characterization of ion ingress into reactive aggregates.

After alkali ions penetrate into the reactive aggregate, they react with the dissolved silica of the aggregate and produce a volume of hydrophilic alkali-silicate gel $V_{gel}(t)$. Detailed description as well as a sensitivity analysis of the model can be found in [5].

3.1 Micromechanics model for ASR induced concrete expansion

The ASR gel is assumed to fill the pore space of the aggregate which is represented in the model by penny shaped microcracks of volume fraction V_c. Gel absorbs the moisture and swells generating a pressure which causes microcracking in the aggregates. Such microcracking is characterized by the growth of the penny shaped cracks [4] and is considered to be controlled by the evolution of the ASR gel volume $V_{gel}(t)$

$$V_c = V_{gel}(t). \quad (12)$$

Here, we assume that the alkali-silicate gel is incompressible [3]. Given the microcrack volume V_c, the rate of crack growth can be identified and the updated size of the microcrack can be found.

Such an evolution of penny shaped microcracks in the aggregates eventually manifests itself as an expansion of the concrete at the structural level. In order to obtain the macroscopic ASR strain due to the microcrack growth in the aggregate, we consider REVs (Representative Elementary Volume) at two scales as depicted in Fig.(6). At the level of concrete the REV is characterized by the cement paste matrix with embedded aggregates of spherical shape. At the level of individual aggregate, the REV is characterized by penny shaped microcracks of radius w and crack width $2c$ ($c \ll w$) embedded in the aggregate. The process of upscaling starting from the propagation of an individual penny shaped microcrack (Fig.(6)d) to the macroscopic scale (Fig.(6)a) is described in detail in [4, 5].

In [4] the mechanisms of microcracking of the aggregate as well as of the cement paste matrix were presented, which correspond to the deterioration processes taking place in the concrete with slowly and rapidly reactive aggregates, respectively. However, in this work we consider microcrack propagation only in the slowly reactive aggregates which were used in the experimental program of the project FOR 1498 [5].

4 ASR EXPANSION IN CONCRETE PAVEMENTS

Here we combine the models described in the previous Sections in order to obtain the strain profile resulting from ASR in a concrete pavement. A 1D simulation is performed where the two boundaries of the domain correspond to the upper and lower surface of the pavement.

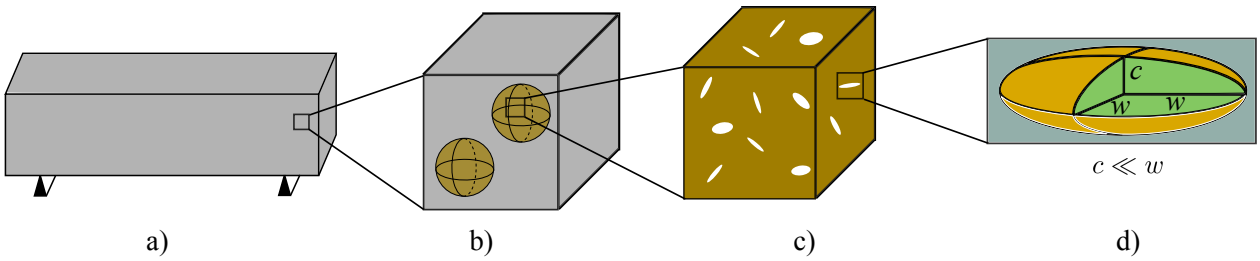

Figure 6: Multiscale characterization of concrete: a) structural level; b) concrete REV (Representative Elementary Volume) consisting of the cement matrix with embedded spherical aggregates; c) cement paste and aggregate REV containing distributed penny-shaped microcracks; d) penny-shaped microcrack [3]

On the upper boundary the Dirichlet boundary condition in the form of the moisture content is applied. The applied values correspond to the environmental conditions measured experimentally in an interval of 3 hours within the period of 1 year. The experimentally obtained boundary conditions for 1 year is sequentially repeated 30 times in order to simulate the environmental conditions for 30 years. At the lower boundary two different conditions imitating two different cases are applied [10]. The first one is the case of a "poor dewatering" meaning that there is always moisture present at the lower surface of the pavement between the concrete layer and the hydraulically bound base layer. The second one is the case of "good dewatering" meaning that the moisture cannot accumulate at the lower surface of the pavement. The initial moisture content as well as the hydraulic conductivity K_s are assumed to be the same in the whole pavement structure, i.e. we do not take into account the increase of the permeability K_s (Fig. 2) due to cracks near the pavement surface.

The presence of de-icing salts on the pavement surface is modelled by applying the respective sodium content at the upper boundary. It is applied within the period of three winter months each year. It must be noted that during the drying part of the cycle, sodium ions remain in concrete and are not transported out of the pavement.

This physical mechanism is taken into account by introducing the following changes into Eq.(10): $a = 0$ for $a < 0$.

The ion and moisture profiles obtained from the simulations were used to determine the ASR expansion profile. Given the profile of sodium ions, the concentration of additional external alkalis in the cement paste can be calculated and accounted for in the right hand side of Eq.(11). This leads to the production of larger amounts ASR gel and consequently to larger ASR induced strains. Ingress of moisture not only contributes to the alkali transport from the pavement surface into the bulk material (i.e. on the macroscale), but also promotes the transport of ions into the aggregate at mesoscale. This is considered by multiplying the aggregate diffusivity in Eq.(11) by a function of the moisture content

$$f(\theta) \quad = \quad \begin{cases} 0, & \theta \leq \theta_{crit} \\ \frac{\theta - \theta_{crit}}{\phi - \theta_{crit}}, & \theta > \theta_{crit} \end{cases} , \quad (13)$$

where θ_{crit} defines the content of moisture below which no ASR is experimentally observed [10]. When the moisture content is below this threshold value, the pore space of the aggregate is not filled with moisture, prohibiting ion diffusion into the aggregate. Using the moisture and ion profiles together with Eq.(11), the spatio-temporal evolution of the ASR gel volume in time and at various depths in the pavement is determined. Finally, applying Eq.(12) and the micromechanics approach described in Section 3.1, the evolution of ASR strain profiles for a period of 30 years can be obtained. The model parameters used for the mesoscale and micromechanics models were chosen and analysed in [5].

4.1 Results

Using the proposed modelling approach, we determine the profiles of ASR expansion in the concrete pavement for two cases representing "good" and "poor dewatering" conditions. Fig.(7) presents the results for the case of "good dewatering".

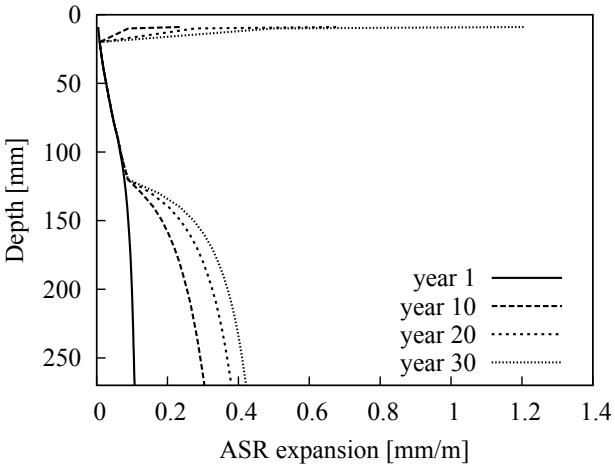

Figure 7: Evolution of ASR induced strain in a concrete pavement obtained for the scenario "good dewatering" after 1, 10, 20 and 30 years.

Fig.(7) reveals that after 30 years, the highest value of ASR strains is reached at the lower and upper surface of the pavement and that the rate of the strain growth decreases with time. The latter can be explained by the evolution of alkali-silica reaction which is characterized by a logarithmic growth of ASR expansion in time [5]. It is noted, that the strain profiles do not follow a linear shape as was assumed in [10]. The region of the relatively high ASR strains at the upper surface of the pavement shown in Fig.(7) is caused by the high moisture content in that region. However, such high values of ASR strain at the upper surface of pavement may be an overestimation. Shrinkage induced cracks at the concrete surface serve as an additional reservoir for the ASR gel.

Also, alkali leaching [6] out of the pavement surface would lead to a reduction of the alkalis near the surface. Both mechanisms are not considered in the presented model. It is also observed that the strains between 2 and 13 $[cm]$ do not increase with time. This effect is the result of the fact that, in this range of depth, the moisture content stays below the threshold according to Eq.(13) during most of the investigated time period of 30 years.

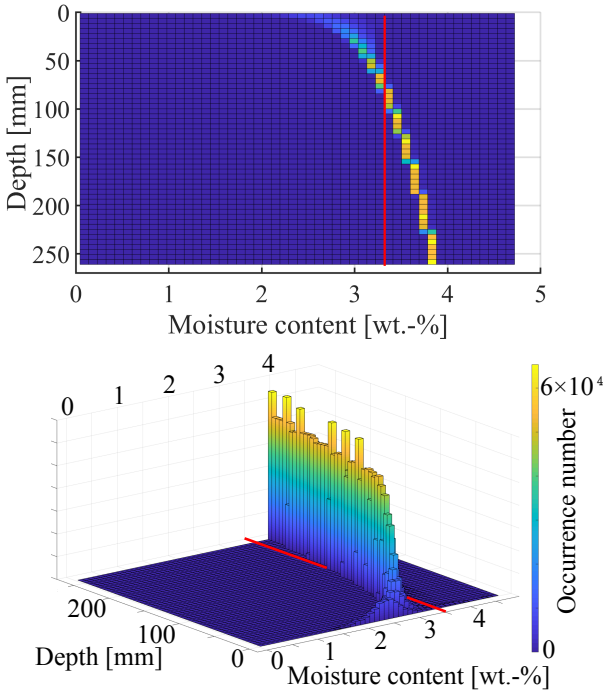

Figure 8: Graphical demonstration of how frequently a particular moisture content occurs at a particular depth under conditions of "good dewatering" up to a period of 30 years. Yellow colours denote the highest occurence frequency, blue colours denote the lowest occurence frequency. Red line denotes the threshold value θ_{crit}.

This is observed in Fig.(8) where the yellow colour denotes high occurrence frequency and blue colour denotes low occurrence frequency of specific moisture content during 30 years at the specific depth. The solid red line depicts the threshold value θ_{crit}. For the case of "poor dewatering" (Fig.(9)) the ASR strains near the lower surface of pavement reach the value of $0.5\,[mm/m]$ in comparison to $0.4\,[mm/m]$ for the case of "good dewatering". In contrast to Fig.(7), the region of low levels of ASR strains in the middle of the pavement is not observed in Fig.(9). This is due to the effect of moisture on ASR gel formation (Fig.(10)).

4.2 Influence of reactive aggregate fraction

From Figs.(7) and (9) it can be concluded that "dewatering" at the lower surface of pavement plays an important role.

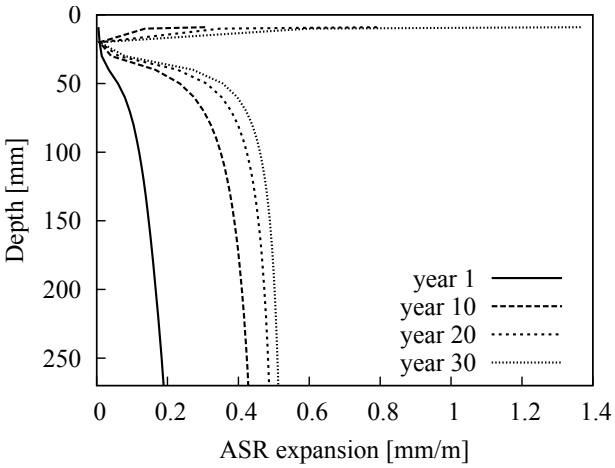

Figure 9: Evolution of ASR induced strain in a concrete pavement obtained for the scenario "poor dewatering" after 1, 10, 20 and 30 years.

Utilization of "good dewatering" reduces ASR strain in the lower region up to 20 [%]. Furthermore, the expansion in the middle part of the pavement is significantly reduced. However, ASR expansion and consequently the material degradation can also be reduced by using non-reactive aggregates. Fig.(11) shows the reduction of the ASR expansion calculated for the case when 50 [%] of the reactive aggregates are replaced by non-reactive aggregates.

5 CONCLUSIONS

In this paper a multiscale approach for the analysis of ASR induced concrete deterioration was presented. The modeling approach takes into account the effect of moisture and ion transport on the evolution of ASR strains at the structural scale using a combination of diffusion-advection models, linear-elastic fracture mechanics, micro-poromechanics and mean-field homogenization. The model is used to to determine the ASR induced evolution of microcracking and strain in a concrete pavement for a period of 30 years

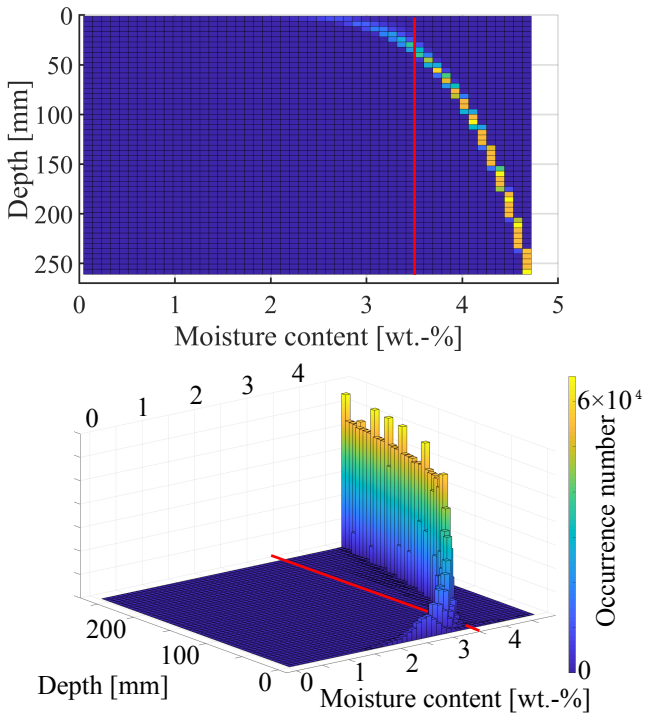

Figure 10: Graphical demonstration of how frequently a particular moisture content occurred at a particular depth under the conditions of "poor dewatering" within the period of 30 years. Yellow colours denote the highest occurence frequency, blue colours denote the lowest occurence frequency. Red line denotes the threshold value θ_{crit}.

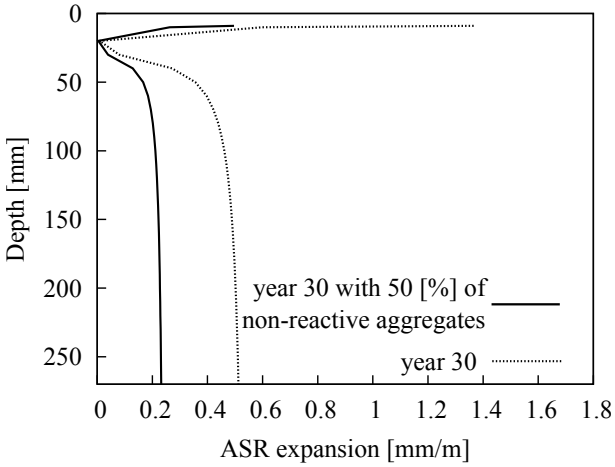

Figure 11: Profiles of an ASR induced strain in the concrete pavement obtained for scenario "poor dewatering" after 30 years. The two curves show the reduction in ASR induced strain when 50 [%] of the reactive aggregates are replaced by the non-reactive ones.

The ASR strain at the bottom surface of the

pavement can be reduced up to 20 [%] if "good" instead of the "poor" dewatering conditions are applied. The dewatering conditions at the lower surface of the pavement also strongly influence ASR induced microcracking and expansion in the centre of the concrete pavement.

6 ACKNOWLEDGEMENTS

This work has been partially supported by the German Research Foundation (DFG) in the framework of Subproject 3 of the DFG-Research Group FOR 1498. This support is gratefully acknowledged.

REFERENCES

[1] V. Baroghel-Bouny, M. Mainguy, T. Lassabatère, and O. Coussy. Characterization and identification of equilibrium and transfer moisture properties for ordinary and high-performance cementitious materials. *Cement and Concrete Research*, 29:1225–1238, 1999.

[2] T. Iskhakov, J.J. Timothy, and G. Meschke. Multiscale modelling of alkali transport and ASR in concrete structures. *Proceedings in Applied Mathematics and Mechanics (PAMM)*, 1, 2018.

[3] T. Iskhakov, J.J. Timothy, and G. Meschke. Multiscale modelling of ASR induced degradation in concrete. In G. Meschke, B. Pichler, and J. Rots, editors, *Computational Modelling of Concrete Structures (EURO-C 2018)*, pages 345–352. CRC Press, March 2018.

[4] T. Iskhakov, J.J. Timothy, and G Meschke. Expansion and deterioration of concrete due to ASR: Micromechanical modeling and analysis. *Cement and Concrete Research*, 115:507–518, 2019.

[5] T. Iskhakov, J.J. Timothy, and G Meschke. From gel formation to concrete expansion: A multiscale analysis of asr. 2019.

[6] S. Multon and A. Sellier. Multi-scale analysis of alkali–silica reaction (asr): Impact of alkali leaching on scale effects affecting expansion tests. *Cement and Concrete Research*, 81:122–133, 2016.

[7] S. Poyet, S. Charles, N. Honoré, and V. L'hostis. Assessment of the unsaturated water transport properties of an old concrete: Determination of the pore-interaction factor. *Cement and Concrete Research*, 41:1015–1023, 2011.

[8] M.T. van Genuchten. A closed-form equation for predicting the hydraulic conductivity of unsaturated soils. *Soil Science Society of America*, 44:892–898, 1980.

[9] F. Weise, E. Krütt, and B. Meng. AKR unter kombinierten einwirkungen - rissbildungs- und transportmechanismen. In H.-M. Ludwig, editor, *Tagungsbericht 20. Internationale Baustofftagung ibausil*, volume 2, pages 93–105, Weimar, 2018. F.A. Finger-Institut fr Baustoffkunde.

[10] A. Wiedmann, E. Kotan, and H.S. Müller. AKR unter kombinierten einwirkungen - schadensrisiko und schadensentwicklung in betonfahrbahnen. In H.-M. Ludwig, editor, *Tagungsbericht 20. Internationale Baustofftagung ibausil*, volume 2, pages 107–114, Weimar, 2018. F.A. Finger-Institut fr Baustoffkunde.

[11] P. Zhang, D. Hou, Q. Liu, Z. Liu, and J. Yu. Water and chloride ions migration in porous cementitious materials: An experimental and molecular dynamics investigation. *Cement and concrete research*, 102:161–174, 2017.